JOURNAL OF PROPULSION AND POWER
Vol. 24, No. 6, November–December 2008

Spanwise Wake and Discrete Jet Disturbances on a Separating Turbine Blade

D. Reimann,* M. Bloxham,* J. Pluim,* and J. Bons†
Brigham Young University, Provo, Utah 84602

DOI: 10.2514/1.32008

Flow velocity and surface pressure measurements were made in a Pack-B low-pressure turbine linear cascade at $Re_c = 20,000$ and 3% inlet freestream turbulence. Under these conditions, the aft-loaded Pack-B (with a peak c_p at 63% c_x) experiences laminar boundary-layer separation on the suction surface near 68% c_x. A wake generator was used to simulate the periodic passing of upstream wakes through the blade passage. The wake passing frequency of 4.5 Hz was set to match a typical engine flow coefficient for a low-pressure turbine ($\phi = 0.85$). A spanwise row of discrete vortex-generating jets located at 59% c_x were also used as a separation control device and were pulsed at a frequency of 5 Hz with a duty cycle of 25%. Data were taken using particle image velocimetry and a hot-film anemometer mounted on a blade-following device. Velocity, turbulence, and intermittency measurements were made along the suction surface of the blade to characterize the bubble dynamics and transitional behaviors for both the presence of unsteady wakes and pulsing vortex generator jets. The wakes caused early breakdown of the separated free-shear layer resulting in a thinning of the separation region. The vortex generator jets caused a near-wall disturbance that was convected downstream, temporarily pushing off the separation bubble. Overall, both wakes and vortex generator jets suppress the size of the steady-state separation bubble, though through different mechanisms. Three-dimensional aspects of the jet disturbance are also discussed.

Nomenclature

B	=	vortex generator jet blowing ratio, $(U_{\text{jet}}/U_{\text{local}})$
c_p	=	pressure coefficient, $(P_{T\text{in}} - P_{\text{local}})/(P_{T\text{in}} - P_{S\text{in}})$
c_x	=	blade axial chord, 0.238 m
F^+	=	dimensionless forcing frequency
f	=	vortex generator jet pulsing frequency, Hz]
L	=	distance between wake generator rods
Re_c	=	Re based on cascade inlet conditions, $c_x U_{\text{in}}/\nu$
S	=	blade spacing
T	=	jet pulsing or wake passing period, s
t	=	time
U	=	velocity magnitude
u	=	instantaneous streamwise velocity component
u_{mean}	=	mean streamwise velocity component
u_{rms}	=	root mean square streamwise velocity component
$\tilde{u}$	=	ensemble-average streamwise velocity
x	=	axial coordinate from the cascade inlet face
y	=	local surface normal coordinate
z	=	spanwise coordinate
Γ	=	intermittency distribution
γ	=	intermittency
ν	=	kinematic viscosity
ϕ	=	$U_{\text{in,axial}}/U_{\text{rod}}$

Subscripts

avg	=	average freestream velocity from vortex generator jet to trailing edge
axial	=	axial direction
in	=	cascade inlet
jet	=	vortex generator jet data set
local	=	local freestream conditions
max	=	maximum value in full cycle
rod	=	wake generator rod
S	=	static
T	=	total
wake	=	wake data set

Presented as Paper 0525 at the 45th AIAA Aerospace Sciences Meeting, Reno, NV, 8–11 January 2007; received 7 May 2007; revision received 18 March 2008; accepted for publication 7 April 2008.

*Research Assistant. Student Member AIAA.
†Associate Professor. Member AIAA.

Introduction

LOW-PRESSURE turbines (LPT) are continually being designed with increased loading for better stage performance. Inherent to increased blade loading is an increased tendency for boundary-layer separation, particularly at low Reynolds numbers when the boundary layers are laminar [1,2]. The LPT environment, which includes high freestream turbulence and the periodic passing of wakes from the previous blade row, also has a very significant impact on the separation dynamics [3–6]. To reduce the losses due to separation, a variety of different passive and active control methods have been studied [7–9]. Many studies are now looking at the effectiveness of control methods in an unsteady environment with the periodic passing of wakes. Of the variety of different methods studied, one that has shown considerable promise is control with vortex-generating jets (VGJs). VGJs are an active control system which have the potential benefit of being able to turn on or off according to their need. Steady VGJ operation induces streamwise vortices which pull high-momentum freestream fluid into the low-momentum separation region and effectively reduce losses due to separation [10–13]. Pulsing VGJs have also shown to be very effective at reducing the separation losses but with a fraction of the mass flow requirements [10]. This makes implementation into a real engine much more practical. For example, Wundrow et al. [14] conducted experiments with pulsed VGJs in a low-speed, multistage compressor. They were successful in manipulating the stage aerodynamics, both favorably and adversely, depending on the duty cycle and amplitude of the pulse. They postulated that, if used properly, the jet pulse can initiate localized mixing and reenergize the boundary layer, thus delaying separation. However, many aspects of the control mechanism for pulsed VGJs are not fully understood. Computational studies by Postl et al. [15] suggest that the primary mechanism for control is boundary-layer transition, whereas Bloxham et al. [16] measured strong streamwise vortices in the pulsed VGJ wake.

Previous work with LPT pulsed flow control has been conducted in steady flow cascades without accounting for the unsteady nature of the flow in an actual engine. Unsteady wakes have been shown to reenergize separation regions as they convect downstream. Stieger et al. [17] attributed this effect to boundary-layer embedded vortical structures. In their linear cascade study of the T106 LP airfoil, they first noted large-amplitude pressure fluctuations as a result of these wake-induced vortical structures. Later, these structures were identified using particle image velocimetry (PIV). Stieger et al. hypothesized that these vortical structures were created by a roll up of the separated shear layer induced by the wake disturbance. Kaszeta et al. [4] also performed a study on the effect of passing wakes on separation in a single passage LPT cascade. They concluded that movement of the separated region during the wake passing could be attributed to three different mechanisms: higher turbulence in the wake, fluctuations in the mean freestream velocity, and subtle changes in the blade incidence angle.

Gostelow and Thomas [18,19] also observed this effect using wake-disturbed flow over a flat plate with an imposed pressure distribution. The pressure distribution was representative of that seen on a compressor blade and encouraged the development of a laminar separation bubble. An upstream rod, parallel with the leading edge of the flat plate, was fastened to a rotating disk. The disk rotated at a rate of 60 rpm, thereby creating two different wakes (one from the rod at an upstream location and the second from a downstream location) every second. Gostelow and Thomas collected their data by traversing a single-element hot wire through the separation bubble at discrete locations. They showed that the wake-induced disturbance stabilized the boundary layer. The wake-induced disturbance was followed by a calmed region that delayed transition and stabilized the boundary layer against separation. This result was further substantiated by similar studies performed by Funazaki et al. [20,21], Cattanei et al. [22], and Zhang and Hodson [7,8].

For the eventual implementation of VGJs into future LPT designs, it is necessary to better understand their influence on the flow dynamics. The effects of the periodic passing of wakes through the flow domain also need to be better understood for future blade designs and the implementation of VGJs. The primary objective of this study is to compare wakes and VGJs as flow control mechanisms. By further understanding each one, their unique benefits may be used and combined together synergistically.

Experimental Setup

A detailed description of the cascade facility used for this study is found in Eldredge and Bons [12]. The open-loop wind tunnel is driven by a centrifugal blower and produces conditioned exit flow with ±2% velocity uniformity and 0.3% freestream turbulence at the cascade inlet. For the present study, this level of background freestream turbulence was augmented to 3% with a passive square-bar grid located 5 axial chords c_x upstream of the cascade. At the cascade inlet plane, the freestream turbulence was fairly isotropic with an integral length scale of 2 cm. Acceleration in the blade passage causes the turbulence level to decay to below 2% at the exit, while the integral length scale increases to nearly 3 cm at the cascade exit plane.

The test section is a two passage cascade containing the Pratt and Whitney Pack-B blade configuration. A depiction of the cascade is found in Fig. 1. The Pack-B blade has an axial chord of 0.238 m, a span of 0.38 m, a design Zweifel coefficient of 1.15, and a cascade solidity of 1.14. At $Re_c = 20,000$, a nonreattaching separation bubble forms on the aft portion of the blade beginning near 68% c_x. The innermost blade in the cascade contains 13 static pressure taps. All c_p and velocity data were taken over the center 0.15 m of blade span, where the flow was confirmed to be approximately two-dimensional. The c_p profile is produced by sequentially connecting these pressure taps to a 0.1 in. H_2O Druck differential pressure transducer referenced to a pitot tube located upstream of the cascade inlet. This differential pressure is then divided by the dynamic pressure at the inlet to yield c_p. The resulting c_p distribution was compared with a prediction generated by the U.S. Air Force Research

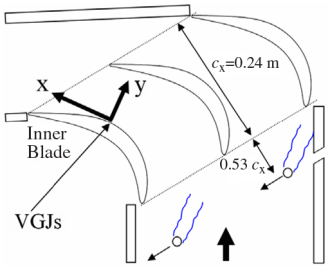

Fig. 1 Three-blade linear cascade with Pack-B blades and upstream wake generator.

Laboratory using a 2-D viscous solver labeled VBI (vane-blade interaction code) in Fig. 2 [23]. Uncertainties in the pressure measurements translate to an uncertainty of ±0.25 in the c_p data at $Re_c = 20,000$. The inlet bleeds and tailboards can be positioned to match both the c_p distribution and the boundary-layer behavior of the eight-blade Pack-B linear cascade used by Sondergaard et al. [24].

The inner blade of the cascade houses a pressure cavity that connects to a spanwise row of vortex generator jets. These jets are 2.6 mm in diameter d and are spaced $10d$ apart along the full span of the blade at 59% c_x. The jets are injected into the flow at a 30 deg pitch angle and a 90 deg skew angle to the flow (see inset of Fig. 3). The pressure cavity is connected to high-pressure air with an inline solenoid valve that regulates the exit velocity of the VGJs. The valve was operated at a frequency of 5 Hz with a duty cycle of 25%, the same conditions studied by Bons et al. [25]. The jet blowing ratio in this study was fixed near $B_{\max} = 2$, where the blowing ratio is defined as the ratio of the jet exit velocity to the local freestream velocity ($U_{\text{jet}}/U_{\text{local}}$). The jet profile was measured as the VGJ exited the blade into a quiescent environment using a single-element hot-film anemometer positioned normal to the jet exit. The resulting jet history plot is presented in Fig. 3. The jet profile is essentially a step function with the initial, high-frequency oscillations attributed to the compressibility of the air in the pressurized cavity.

A wake generator is placed 12.7 cm (0.53 c_x) upstream of the cascade inlet (Fig. 1). Unsteady wake disturbances are created using 4-mm-diam carbon fiber rods. The rods are oriented in the spanwise direction and are drawn through the tunnel on a chain sprocket system driven by a variable frequency motor. Low-density foam is used at both the tip and base of the rods to dampen vibrations and seal the tunnel. An optical sensor detects the passage of the rods as they exit the tunnel. The speed of the rods was adjusted to maintain a normalized velocity of $U_{\text{rod}}/U_{\text{in}} = 1.05$ (flow coefficient $\varphi = 0.85$) with a fluctuation of approximately ±2%. The period between rods was measured to be 225 ms, which is very close to the VGJ pulsing period of 200 ms. The dimensionless forcing frequencies are $F^+ = 0.24$ and 0.27 for the wake and rod disturbance, respectively. The rods are spaced at $L/S = 1.64$, where L is the distance between the rods and S is the blade spacing. The larger spacing between rods (compared to the cascade spacing) is intended to simulate vane wakes impinging on a rotor blade row because the vane count is typically 60–75% of the blade count for a given LPT stage.

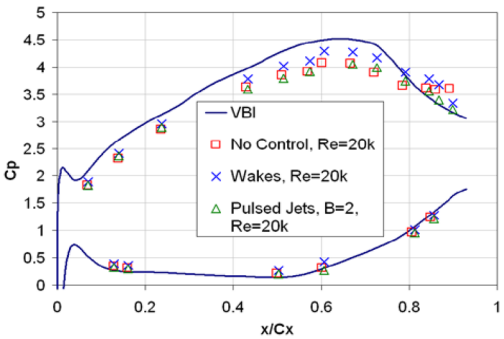

Fig. 2 Pressure coefficient c_p distributions along the Pack-B at $Re = 20,000$ without control, with wakes, and with VGJs as compared with VBI prediction at high Re (nonseparating).

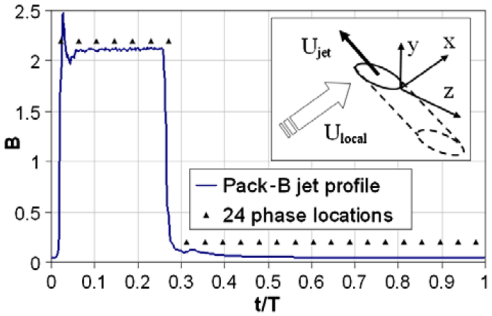

Fig. 3 VGJ pulse history with phase markings and inset diagram of VGJ orientation.

The primary tool for flow diagnostics was a single-element hot-film anemometer mounted to a three-axis traverse located atop the cascade. The hot-film element has a diameter of 50.8 μm, a length of 1.02 mm, and a maximum frequency response of roughly 8 kHz. The traverse incorporated a blade-following device that allowed data to be taken at constant wall distance spanning most of the blade suction surface (from 30% c_x to the blade trailing edge). Seventeen streamwise profiles were obtained with wall distances approximately evenly spaced between 1.2 and 20 mm. The uncertainty in velocity was ± 0.05 m/s, and the follower y position was accurate to within ± 0.2 mm. Each profile consisted of 64 streamwise measurement locations, with a spacing ranging between 2.7 and 6.9 mm, the smaller steps concentrated in the region of the separation bubble.

Data were also taken using a single-camera LaVision PIV system mounted to a three-axis traverse below the test section. A Nd:YAG laser was used to project two consecutive 1-mm-thick laser sheets (with a 250 μs time separation) in the x–y plane into the test section (see inset of Fig. 3 for coordinate system). The flow was seeded with olive oil particles having diameters between 1 and 2 μm. The high-speed digital camera positioned below the test section had a resolution of 1376 × 1040 pixels. According to LaVision [26], the uncertainty in the seed particle displacement is approximately 0.2 pixels. Coupled with a 95% confidence interval estimate of the uncertainty in the freestream velocity, the total uncertainty is 3%. The data acquired for this study were all phase averaged from 40 individual vector fields. Measurements were taken in 18 spanwise z locations for the VGJ conditions and 6 spanwise locations for the wake data. Data at fewer spanwise locations were taken for the wake data due to the anticipated 2-D influence of the wakes on the separation bubble. The z locations for both jet and wake conditions spanned one VGJ hole pitch ($10d$). The first z location was taken directly below a midspan VGJ, where the flow was shown to be spanwise uniform. Subsequent levels were taken by traversing toward the top of the test section in the negative z direction according to the right-hand rule (x is the flow direction and y is normal to the blade surface). The single-camera data set required two different test windows to capture flow in the desired region of the blade. These windows covered an upstream (~50– ~ 81% c_x) and a downstream (~80– ~ 100% c_x) portion of the blade with approximately 6 mm of overlap. The data windows were later merged together to create a continuous set of data, as depicted in Fig. 4. It should be noted that all

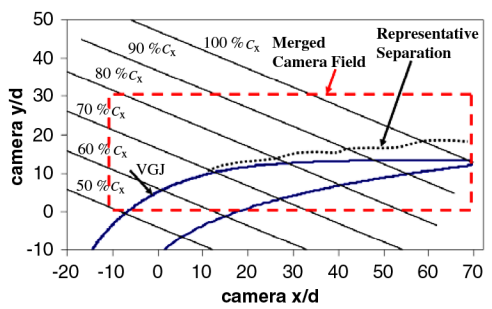

Fig. 4 Upstream/downstream PIV data collection regions (only part of the total blade profile).

of the PIV data are presented in the camera coordinate system. In the region of interest (59–100% axial chord), the blade suction surface is relatively flat. The result is that the y coordinate of the camera is approximately surface normal in this region.

Data Processing

Because the goal of this study was to document transition-related phenomena, large data records were taken at each position to assure steady statistics. Flow intermittency γ was calculated using the methodology developed by Volino et al. [27], which employs both the first and second velocity derivatives as turbulence discriminators. The data are initially high-pass filtered to eliminate low-frequency fluctuations that are common to both laminar and turbulent zones. Then, the absolute value of the first derivative of velocity is compared with a predetermined threshold based on the local velocity fluctuations. This procedure yields a $\Gamma_1(t)$ distribution, which is the first intermittency discriminator. A second discriminator Γ_2, based on the absolute value of the second derivative of velocity, is then coupled with the first discriminator to yield a final intermittency value. The composite result is low-pass filtered to eliminate erratic transitions between the two states. The only modification that was made to the original Volino formulation was to calculate the high- and low-pass filter frequencies using the local mean velocity, rather than the local freestream velocity U_{local}. By doing this, the cutoff frequencies are more directly tied to the local convective speed of flow disturbances over the hot-film anemometer.

At each measurement location, the data acquisition time was 24 s measured at a frequency of 10 kHz. The transistor–transistor logic signal from the pulsed valve controller was used to phase-lock the data acquisition for the pulsed VGJ control case, whereas the rod sensor signal was used for the wake data. The data processing methodology shown schematically in Fig. 5 was followed for both data sets, though it is described here for the VGJ case only.

The cycle count and phase length are slightly different for the wake data because the periods are different ($T_{\text{wake}} = 225$ ms, whereas $T_{\text{jet}} = 200$ ms). First, the 120 cycles (24 s × 5 Hz) of velocity data were averaged to produce an ensemble-average mean velocity distribution $\tilde{u}$ at each point. This ensemble was then subtracted from each of the 120 cycles to eliminate the bulk unsteady motion of the flow from the statistical calculations. The resulting velocity record represents cycle-to-cycle deviations from the ensemble-average mean flow. The next step was to divide each cycle into 24 phases of equal length (8.3 ms). The first phases of data from all 120 cycles were then concatenated together to form a continuous velocity deviation signal ($u - \tilde{u}$) associated with the first 8.3 ms of jet actuation (a total of 10,000 data points). This data record was evaluated to determine intermittency for that phase. The process was repeated for each of the 24 phases to produce the time variation of intermittency over one complete pulsing cycle.

Results

The pressure coefficient c_p distributions for the Pack-B blade are presented in Fig. 2. The figure includes experimental data for the uncontrolled case, for the presence of wakes, and for the controlled case with pulsed jets, all at $Re_c = 20,000$. It can be seen that, for the baseline uncontrolled case, the c_p values plateau by 80% axial chord,

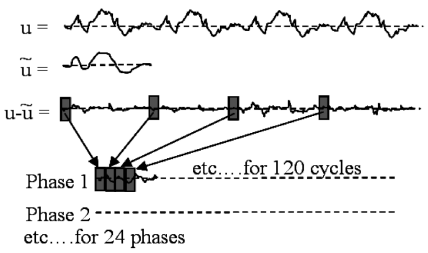

Fig. 5 Data processing flowchart for phase-locked unsteady velocity data from hot-film anemometer.

which is indicative of boundary-layer separation. In the presence of unsteady wakes, the c_p values deviate from the inviscid prediction due to the lower Reynolds number, but do not plateau as the uncontrolled case does. The c_p data with the pulsing jet follow the uncontrolled c_p distribution very closely until 80% axial chord, when the pulsing jet c_p values drop down near the VBI prediction, indicating a reattachment of the separated region.

PIV data were collected for both the wake and VGJ disturbance conditions. Forty image pairs of velocity were averaged at multiple locations along the pitch spanning two VGJ holes. The PIV images were phase locked at different times throughout the disturbance period. Isovelocity surfaces were then created from the velocity data at each phase. Figure 6 contains isovelocity surfaces for $U/U_{\text{in}} = 0.75$ for the wake and jet data. The flow moves from right to left as depicted by the black arrow. The curvature of the turbine blade has been removed from the surface to isolate the separation region (elevated surface). The isovelocity surfaces are from the dimensionless times t/T_{wake} of 0.11, 0.44, 0.51, and 0.78 for the wake data, and t/T_{jet} of 0.23, 0.48, 0.60, and 0.85 for the VGJ data. The coloring corresponds to the local distance from the isovelocity surface to the blade wall. Each figure also includes either a depiction of the jet velocity profile (the black arrow indicates t/T_{jet} position) or the approximate wake location in the passage (represented by gray dashed lines, per Wu and Durbin [28]). For the wake data set, the isovelocity surface of $t/T_{\text{wake}} = 0.11$ shows the separation region before the impact of the wake disturbance. Subsequent surfaces of t/T_{wake} show the effect of the wake disturbance on the separation bubble. The wake disturbance has a very two-dimensional effect as there is little spanwise variation. By contrast, the jet disturbance initially has a three-dimensional effect as it penetrates the upstream end of the separation region (as shown by the isovelocity surfaces of $t/T_{\text{jet}} = 0.23$ and 0.48 in Fig. 6a). The isovelocity surface of $t/T_{\text{jet}} = 0.48$ depicts the evolution of the initial three-dimensional effect to a two-dimensional effect that is then ejected from the blade. This is further shown in the surfaces of $t/T_{\text{jet}} = 0.60$ and 0.85.

As a means of studying the differences between the wake influence and the VGJ influence on the separation bubble in more detail, phase-locked velocity data were taken with a hot-film anemometer at a single midspan location about 2 jet hole diameters above one of the VGJ holes ($z/d = 6$ in Fig. 6). Phase-locked plots of mean velocity normalized by the inlet velocity are shown in Fig. 7. Of the 24 phases, every odd phase is displayed in Fig. 7 for both the wake and the VGJ data sets. In the upper right-hand corner of each contour plot is the nondimensional time value t/T_{wake} for the wake plots and t/T_{jet} for the VGJ plots.

The extent and location of the wake can be seen in both the $U_{\text{mean}}/U_{\text{in}}$ plots of Fig. 7a and the corresponding $U_{\text{rms}}/U_{\text{in}}$ plots of Fig. 8a. The wake enters the data domain near $t/T_{\text{wake}} = 0.19$, and its influence can be seen until about $t/T_{\text{wake}} = 0.69$ (as indicated by the white arrow). As the wake impacts the separated region, it

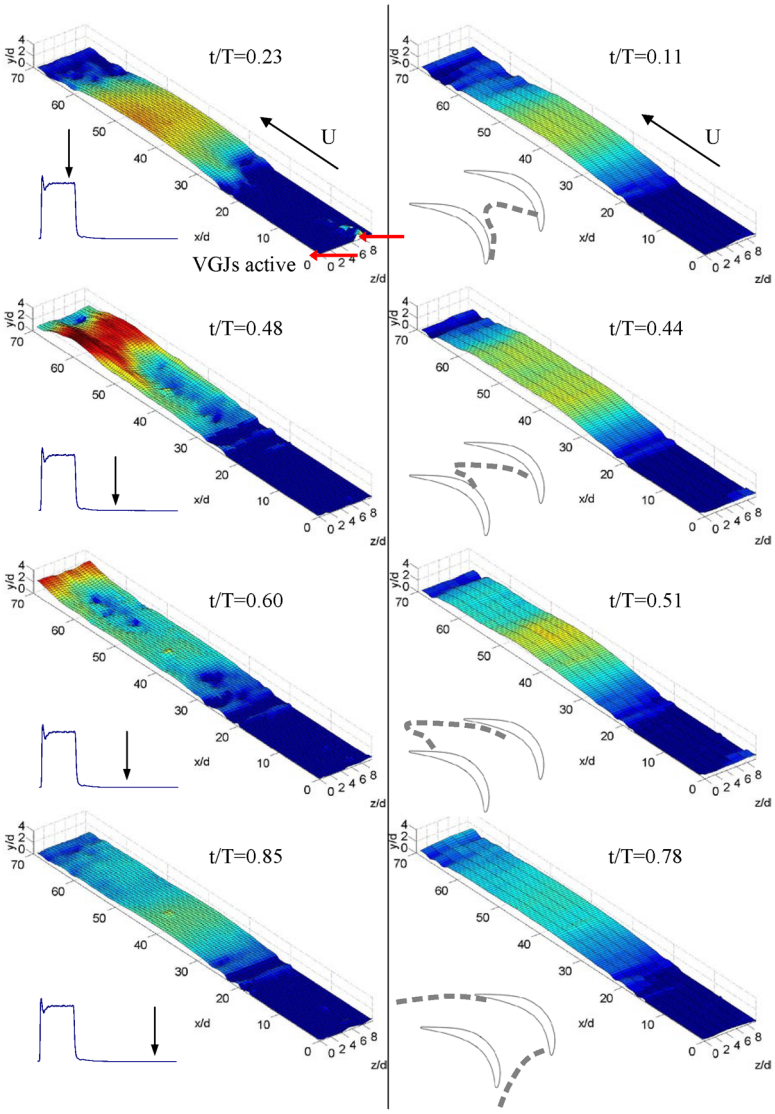

a) Jets only (5Hz, 25% duty cycle) **b) Wake only**

Fig. 6 Phase-locked isovelocity surfaces ($U/U_{\text{in}} = 0.75$) for jet and wake conditions.

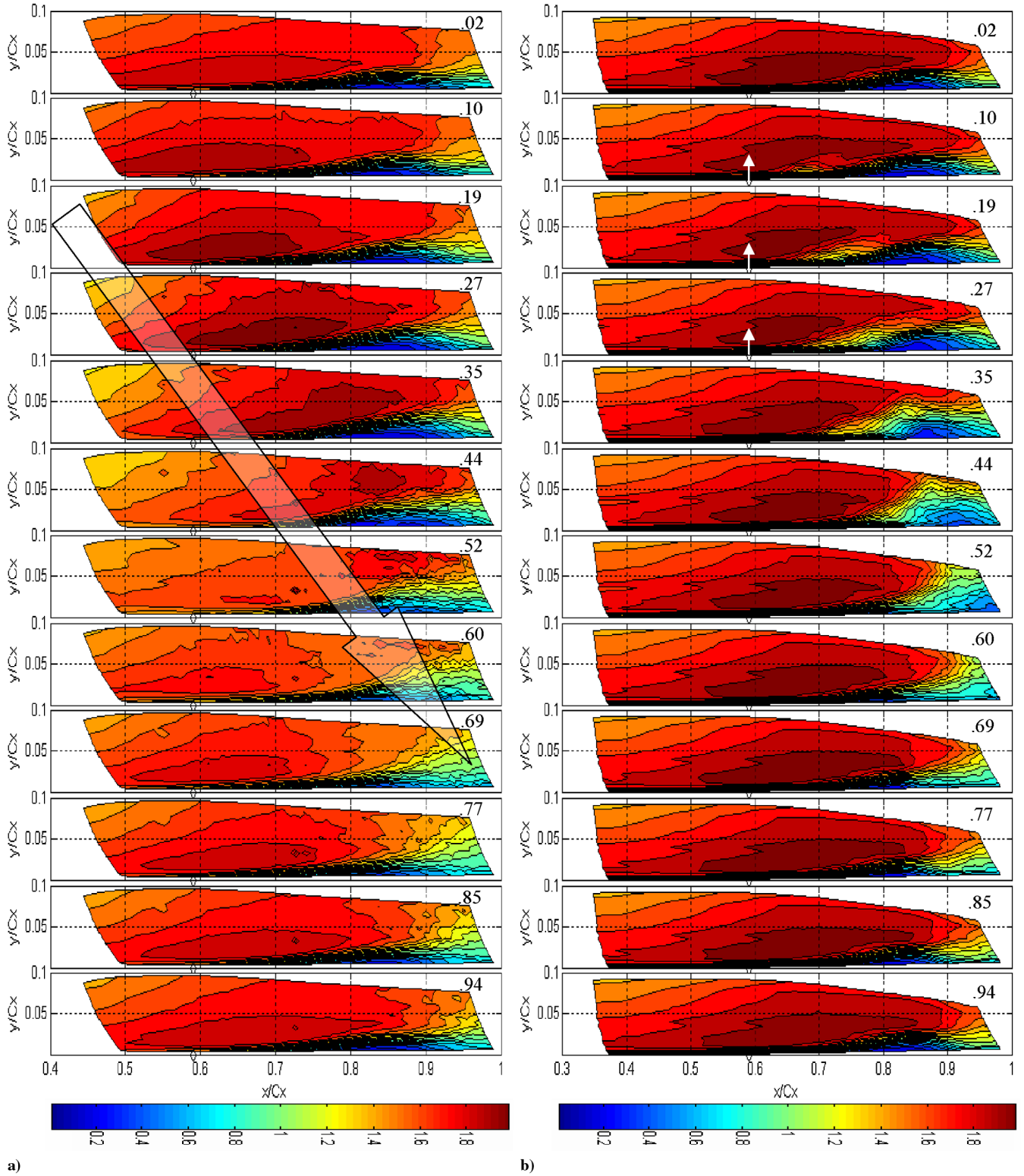

Fig. 7 Phase-locked contour plots of $U_{\text{mean}}/U_{\text{in}}$ for a) wake and b) VGJ conditions at $z/d = 6$, with white arrows indicating VGJ on times.

significantly reduces the size of the separation bubble by increasing the level of mixing. Elevated mixing across the separated shear layer increases the apparent shear stress on the separated fluid, effectively thinning, but never completely eliminating, the separation. After the wake passes, the residual separation bubble again increases in size before it is impacted by the next wake.

The influence of the VGJ on the separation bubble can be seen in Fig. 7b. The jet pulse initiates immediately after $t/T_{\text{jet}} = 0.02$ and ends just after $t/T_{\text{jet}} = 0.27$ (note white arrows). The pulse influence can be seen upstream of the separation bubble from $t/T = 0.10$–0.35. This near-wall jet disturbance enhances mixing locally and produces a higher mean momentum at the upstream end of the separation bubble. Because the upstream end convects more quickly, it catches up with the bulk of the separation region, yielding a thickening near $0.88 < x/c_x < 0.95$ as low-momentum fluid accumulates. This separated region subsequently convects off the trailing edge of the blade. As the separation region is being pushed off the blade, a new separation bubble begins to form and regrow. The accumulation and convection of the separation bubble can also be seen in the isovelocity surface plot of Fig. 6.

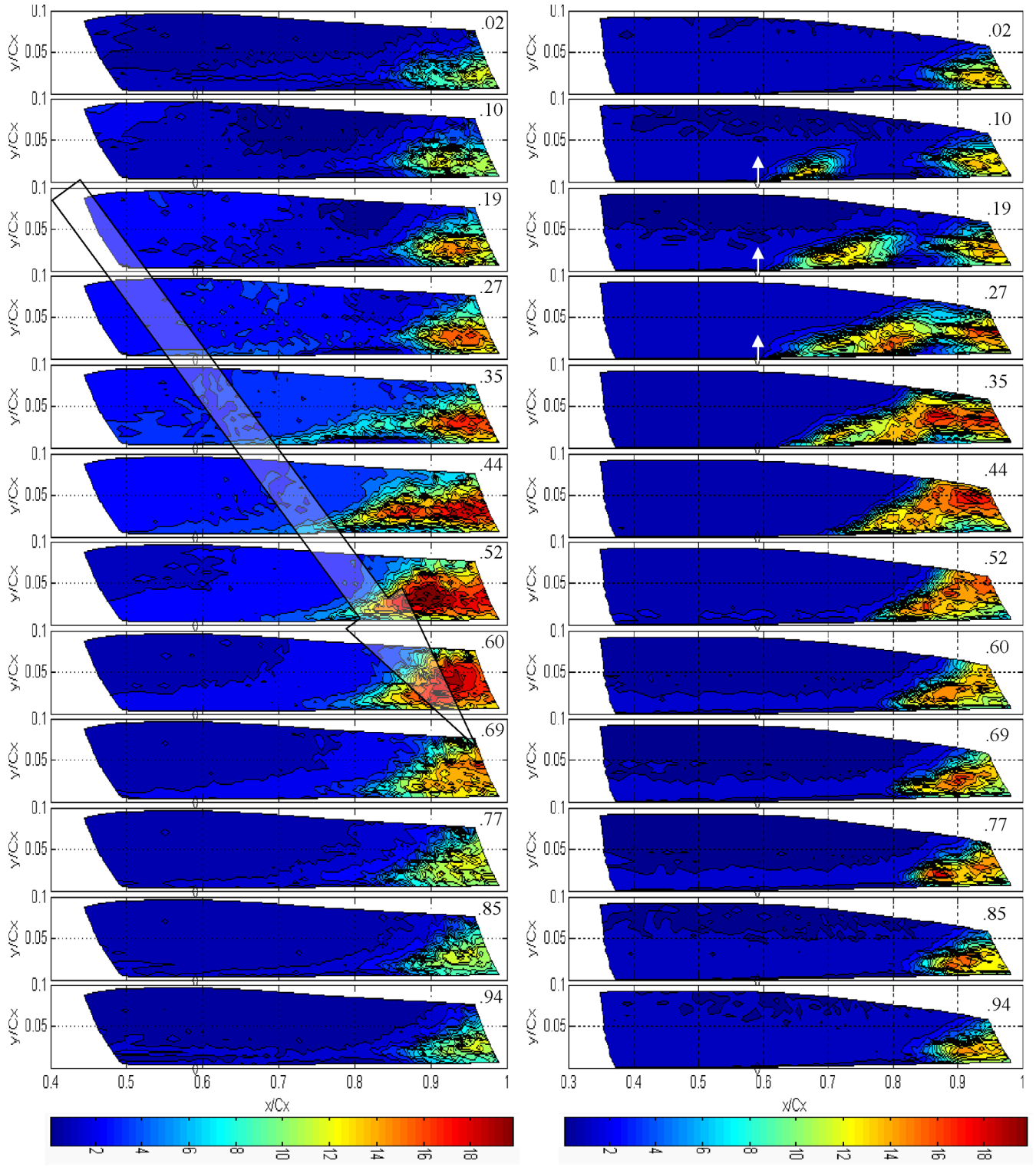

Fig. 8 Phase-locked contour plots of $U_{\text{rms}}/U_{\text{in}}$ for a) wake and b) VGJ conditions at $z/d = 6$, with white arrows indicating VGJ on times.

Evidence of the control mechanisms for both the wake and the VGJ data can be seen in the contour plots of $U_{\text{rms}}/U_{\text{in}}$ in Fig. 8. Again, every odd phase is displayed, showing 12 of the 24 phases for both cases. The natural breakdown of the separated free-shear layer can be seen by the elevated U_{rms} levels off the wall at $y/c_x \sim 0.02$ in both the wake and the jet data at around 85% c_x before the wake or jet influence arrives ($t/T = 0.02$–0.10). The turbulent disturbance of the wake causes unsteadiness and rapid bypass transition of the separated shear layer all the way up near 70% c_x by $t/T_{\text{wake}} = 0.35$. A slight increase in U_{mean} in advance of the lower momentum rod wake is evident in Fig. 7a, from $t/T = 0.19$–0.44. The temporal diffusion brought about by the passing of this high-momentum fluid contributes to destabilization of the separated shear layer and the upstream movement of transition. Similar features were reported by Kaszeta et al. [4] and Jiang and Simon [5] who noted that the wake disturbance moved both the separation and transition locations upstream. Not only does the wake induce early breakdown of the shear layer but also it causes elevated levels of turbulence over the separated region. Even though the turbulent breakdown of the shear layer reduces the separation size, it does not fully eliminate it. The

separated region below the shear layer can still be seen as a thin zone of low turbulence underneath the shear layer, even as the wake is passing over it at t/T of 0.35 and 0.44. As the wake continues off the blade, it leaves behind levels of relatively low turbulence. Gostelow and Thomas [18,19] refer to this region of low turbulence as a "calmed zone" and also show evidence of this wake-induced bypass transition [17]. Whereas the wake influence on the separation bubble starts in the free-shear layer, the vortex generator jet introduces high levels of near-wall turbulence upstream of the separation bubble ($t/T_{\text{jet}} = 0.10$). As the highly turbulent influence of the jet convects downstream, it stays close to the wall and impacts the upstream end of the separation bubble, causing it to accelerate and convect off the blade. A new separation bubble begins to form as soon as the old bubble leaves. For the VGJ case, the residual levels of turbulence in the shear layer never drop as low as the calmed region seen after the passing of the wake.

To explore the three-dimensional nature of the pulsed VGJ flow, a second set of follower data were taken at an elevation of $z/d = 2.7$. Intermittency contour plots for both $z/d = 2.7$ and $z/d = 6$ elevations are included in Fig. 9 at $t/T_{\text{jet}} = 0.10$ and 0.31. The jet influence is noticeable by the abrupt transition at the $z/d = 2.7$ plane, about one phase after it can be seen in the $z/d = 6$ plane. As evidenced in Fig. 9a, the jet trajectory crosses the $z/d = 2.7$ elevation further downstream than at the $z/d = 6$ elevation due to the freestream entrainment of the jet fluid. The jet fluid is also further from the blade surface than at the $z/d = 6$ elevation due to the 30 deg pitch of the VGJ. By $t/T_{\text{jet}} = 0.31$ (Fig. 9b), the jet influence has already impacted the separation region. However, at $z/d = 6$, the jet acts as a near-wall influence, accelerating the separation bubble off the back of the blade. At $z/d = 2.7$, the jet impacts the separation region further away from the blade surface. As a result, the jet, in addition to causing acceleration and convection of the separation bubble, causes unsteadiness in the free-shear layer, resulting in shear-layer breakdown similar to the wake influence. This can be seen in Fig. 9b. After the jet has turned off, the jet's influence on the separation region quickly becomes spanwise uniform as the separation along the entire blade span is reduced and begins to reform (Fig. 6).

For the $z/d = 6$ plane, time-space plots of $U_{\text{mean}}/U_{\text{in}}$, $U_{\text{rms}}/U_{\text{in}}$, and intermittency were created at an elevation of 6.2 mm ($y/c_x = 0.026$) off the wall for both wake and VGJ conditions (Figs. 10–12, respectively). As the bubble is suppressed in both cases, regions of previously low velocity along the aft portion of the blade ($0.8 < c_x < 0.97$) increase in velocity, reaching magnitudes of

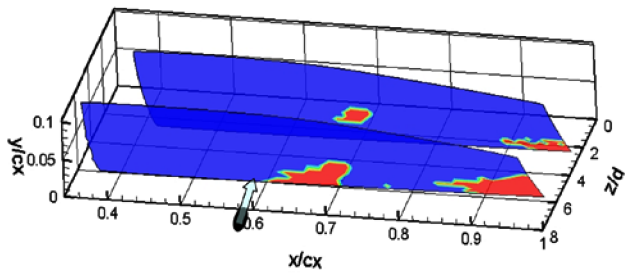

a) t/T$_{\text{jet}}$=0.10 (VGJ on)

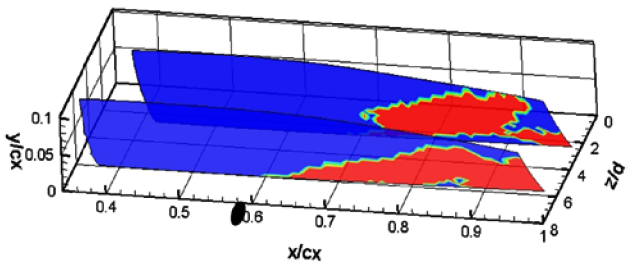

b) t/T$_{\text{jet}}$=0.31 (VGJ off)

Fig. 9 Intermittency plots at a) $t/T_{\text{jet}} = 0.10$ and b) $t/T_{\text{jet}} = 0.31$ at elevations $z/d = 6$ and $z/d = 2.7$.

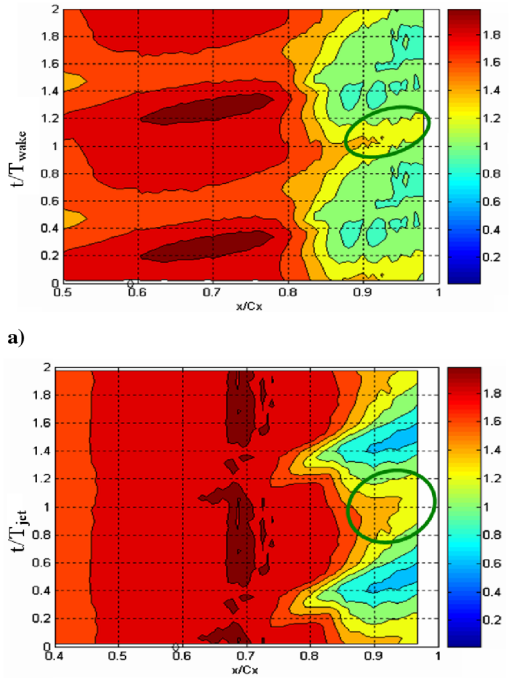

a)

b)

Fig. 10 Time-space contour plots of $U_{\text{mean}}/U_{\text{in}}$ for a) wake and b) VGJ conditions ($z/d = 6$) 6.2 mm from blade surface.

$U_{\text{mean}}/U_{\text{in}} > 1.2$ at $z/d = 6$ and $U_{\text{mean}}/U_{\text{in}} > 1.4$ at $z/d = 2.7$ (not shown). The amount of time that the flow is able to maintain this elevated velocity is greater for the jets compared with the wake disturbance. This region is highlighted in Figs. 10a and 10b by the green ovals. The jet influence maintains this higher velocity for nearly twice as long as the wake disturbance at this y/c_x elevation. Again, this is consistent with previous discussion indicating that the wake produces a gradual thinning of the separation bubble while the jet accelerates the bubble off the blade.

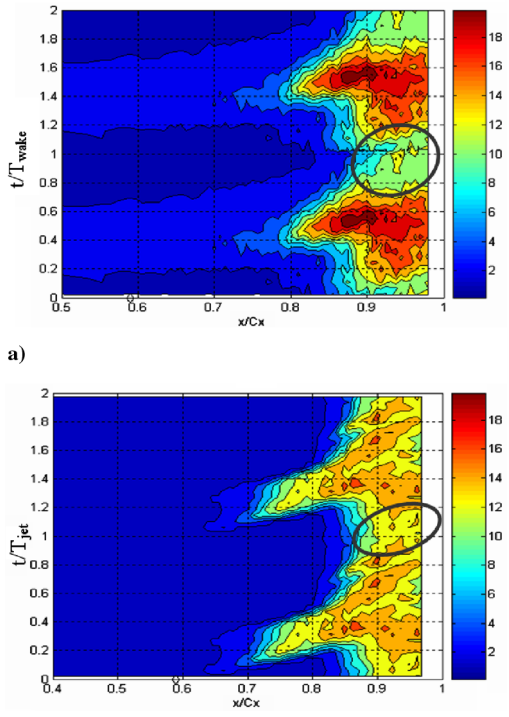

a)

b)

Fig. 11 Time-space contour plots of $U_{\text{rms}}/U_{\text{in}}$ for a) wake and b) VGJ conditions ($z/d = 6$) 6.2 mm from blade surface.

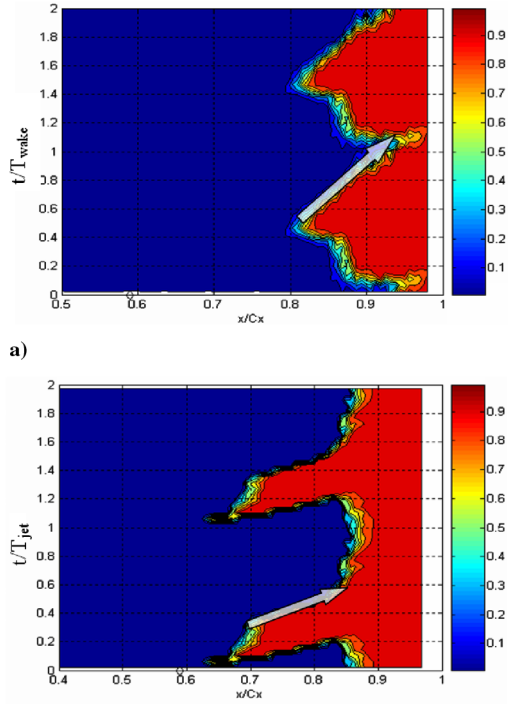

Fig. 12 Time-space contour plots of intermittency for a) wake and b) VGJ conditions ($z/d = 6$) 6.2 mm from blade surface.

Because these time-space plots are at a wall distance within the shear layer, it is easy to see how the wake influences the shear layer differently than the jet. In Fig. 11, much higher levels of turbulence occur from the wake influence as it amplifies the unsteadiness of the free-shear layer. The jet influence does not have a comparable amplifying effect on the free-shear layer at either the $z/d = 6$ or the $z/d = 2.7$ elevations. The region of low turbulence after the disturbance passes, or a calmed zone, is greater and lasts longer due to the passing of the wake than it does due to the passing of the jets at $z/d = 6$. This region has been highlighted by black ovals in Fig. 11.

From the (unfiltered) intermittency time-space plots of Fig. 12 at $z/d = 6$, it can be seen that transition happens rapidly for both the wake and the jet conditions as evidenced from the very narrow transition bands. As the wake starts to impact the separation region near $t/T = 0.4$, the location of transition quickly jumps from near 86% to about 81% c_x. However, the location of transition subsequently moves down the blade much more slowly from the wake influence than it does due to the jet influence. These trajectories are highlighted by the transparent white arrows. The migration velocity of the transition location due to the jet disturbance is close to 2 times that of the wake disturbance at this elevation. The transition location due to the jet ultimately stops at around 85% c_x and remains there until the jet is pulsed again. At $z/d = 2.7$ (not shown), the transition continues downstream to nearly 95% c_x (much like the wake effect) before moving back upstream to about 90% c_x before the next jet impact. The transition location due to the wake migrates down beyond 94% c_x in the calmed zone before quickly moving back to a "steady-state" upstream location around 86% c_x before the impact of the next wake. The data in these figures suggest that VGJs could perhaps be synchronized together with the wakes to achieve even greater separation reduction with an extended calmed zone.

Conclusions

Hot-film and PIV measurements were taken in a low-speed, low-pressure turbine cascade to obtain detailed, unsteady velocity data in the presence of periodic unsteady wakes and pulsing vortex-generating jets. Comparisons were made between the separation characteristics as well as the control characteristics for both cases. In the presence of unsteady wakes, the separation bubble is reduced in size as the wake passes over. This is caused by the unsteadiness found in the wake which triggers early transition of the separated shear layer. The effect of the wake disturbance propagates down toward the wall, reducing the separation size as long as the wake is passing over. As the wake leaves, a calmed region of low-turbulence flow is left behind.

The VGJ influence varies considerably across the hole pitch. Very near the injection location, the VGJ causes a 3-D near-wall disturbance which convects downstream and impacts the separation bubble. The upstream end of the bubble then accelerates downstream faster than the bulk of the low-momentum separated fluid. This creates an accumulation of the separated fluid into a low-momentum mass that subsequently convects off the trailing edge of the blade. As the separation bubble is pushed off the blade, a new separation bubble begins to form and continues to grow until the impact of the next jet. In essence, the VGJ acts as a near-wall source for turbulent transition which convects downstream impacting the separation zone. Further away from the jet injection, the jet fluid is more removed from the wall when it impacts the separation, causing early shear-layer breakdown similar to the wake. Detailed three-component PIV measurements by Bloxham et al. [29] show evidence of vortices as well, but these are thought to have a secondary effect on separation dynamics. The results from this study show promise for the synchronization of VGJs and wakes to achieve synergistic benefits.

Acknowledgments

Financial support from the U.S. Air Force Office of Scientific Research is gratefully acknowledged, with Rhett Jefferies as program manager. Also, this work could not have been accomplished without the help of Katie Crapo George.

References

[1] Matsunuma, T., Abe, H., Tsutsui, Y., and Murata, K., "Characteristics of an Annular Turbine Cascade at Low Reynolds Numbers," International Gas Turbine Inst. Paper 98-GT-518, 1998.

[2] Sharma, O., "Impact of Reynolds Number on LP Turbine Performance," *Proceedings of 1997 Minnowbrook II Workshop on Boundary Layer Transition in Turbomachines*, NASA CP-1998-206958, 1998.

[3] Ozturk, B., and Schobeiri, M. T., "Effect of Turbulence Intensity and Periodic Unsteady Wake Flow Condition on Boundary Layer Development, Separation, and Re-Attachment over the Separation Bubble Along the Suction Surface of a Low Pressure Turbine Blade," *ASME Turbo Expo 2006: Power for Land, Sea and Air*, American Society of Mechanical Engineers Paper GT2006-91293, 2006.

[4] Kaszeta, R. W., Simon, T. W., and Ashpis, D. E., "Experimental Investigation of Transition to Turbulence as Affected by Passing Wakes," *ASME Turbo Expo 2001: Power for Land, Sea and Air*, American Society of Mechanical Engineers Paper 2001-GT-0195, 2001.

[5] Jiang, N., and Simon, T. W., "Transition in Low-Pressure Turbines: Effects of Unsteady Acceleration and Turbulence Intensity," *Journal of Thermophysics and Heat Transfer*, Vol. 19, No. 2, April–June 2005, pp. 148–155. doi:10.2514/1.9954

[6] Funazaki, K., Tetsuka, N., and Tanuma, T., "Effects of Periodic Wake Passing upon Aerodynamic Loss of a Turbine Cascade, Part II," *1999 International Gas Turbine and Aeroengine Congress and Exposition*, American Society of Mechanical Engineers Paper 99-GT-94, 1999.

[7] Zhang, X., and Hodson, H., "The Combined Effects of Surface Trips and Unsteady Wakes on the Boundary Layer Development of an Ultra-High-Lift LP Turbine Blade," *ASME Turbo Expo 2004: Power for Land, Sea, and Air*, American Society of Mechanical Engineers Paper GT2004-53081, 2004.

[8] Zhang, X., and Hodson, H., "Separation and Transition Control on an Aft-Loaded Ultra-High-Lift LP Turbine Blade at Low Reynolds Numbers: Low-Speed Investigation," *ASME Turbo Expo 2005: Power for Land, Sea, and Air*, American Society of Mechanical Engineers Paper GT2005-68892, 2005.

[9] Rivir, R. B., Sondergaard, R., Bons, J. P., and Lake, J. P., "Passive and Active Control of Separation in Gas Turbines," *AIAA Fluids 2000*, AIAA Paper 2000-2235, 2000.

[10] Bons, J. P., Sondergaard, R., and Rivir, R. B., "The Fluid Dynamics of LPT Blade Separation Control Using Pulsed Jets," *Journal of Turbomachinery*, Vol. 124, Jan. 2002, pp. 77–85. doi:10.1115/1.1425392

[11] Volino, R. J., "Separation Control on Low-Pressure Turbine Airfoils Using Synthetic Vortex Generator Jets," *Proceedings of ASME Turbo Expo 2003: Power for Land, Sea, and Air*, American Society of Mechanical Engineers GT2003-38729, 2003.

[12] Eldredge, R. G., and Bons, J. P., "Active Control of a Separating Boundary Layer with Steady Vortex Generating Jets: Detailed Flow Measurements," *AIAA Aerospace Sciences Meeting*, AIAA 2004-751, 2004.

[13] Hansen, L. C., and Bons, J. P., "Time-Resolved Flow Measurements of Pulsed Vortex-Generator Jets in a Separating Boundary Layer," *Journal of Propulsion and Power*, Vol. 22, No. 3, 2006, 2004, pp. 558–566. doi:10.2514/1.13820

[14] Wundrow, D. W., Braunscheidel, E. P., Culley, D. E., and Bright, M. M., "Separation Control in a Multistage Compressor Using Impulsive Surface Injection," NASA TM 2006-214361, 2006.

[15] Postl, D., Gross, A., and Fasel, H. F., "Numerical Investigation of Low-Pressure Turbine Blade Separation Control," AIAA Paper 2003-0614, 2003.

[16] Bloxham, M., Reimann, D., Crapo, K., Pluim, J., and Bons, J. P., "Synchronizing Separation Flow Control with Unsteady Wakes in a Low-Pressure Turbine Cascade," *2007 IGTI Conference*, International Gas Turbine Inst. Paper GT2007-27529, May 2007.

[17] Stieger, R., Hollis, D., and Hodson, H., "Unsteady Surface Pressures Due to Wake Induced Transition in a Laminar Separation Bubble on a LP Turbine Cascade," *Proceedings of ASME Turbo Expo 2003: Power for Land, Sea, and Air*, American Society of Mechanical Engineers Paper GT2003-38303, 2003.

[18] Gostelow, J. P., and Thomas, R. L., "Response of a Laminar Separation Bubble to an Impinging Wake," *Proceedings of ASME Turbo Expo 2003: Power for Land, Sea, and Air*, American Society of Mechanical Engineers Paper GT2003-38972, 2003.

[19] Thomas, R. L., and Gostelow, J. P., "The Pervasive Effect of the Calmed Region," *Proceedings of ASME Turbo Expo 2005: Power for Land, Sea and Air*, American Society of Mechanical Engineers Paper GT2005-69125, 2005.

[20] Funazaki, K., Wakita, Y., and Otsuki, T., "Studies on Bypass Transition of a Boundary Layer Subjected to Localized Periodic External Disturbances," *Proceedings of ASME Turbo Expo 2004: Power for Land, Sea, and Air*, American Society of Mechanical Engineers Paper GT2004-53305, 2004.

[21] Funazaki, K., and Koyabu, E., "Studies on Wake-Induced Bypass Transition of Flat-Plate Boundary Layers Under Pressure Gradients and Free-Stream Turbulence," *Proceedings of ASME Turbo Expo 2006: Power for Land, Sea and Air*, American Society of Mechanical Engineers Paper GT2006-91103, 2006.

[22] Cattanei, A., Zunino, P., Schroder, T., Stoffel, B., and Matyschok, B., "Detailed Analysis of Experimental Investigations on Boundary Layer Transition in Wake Disturbed Flow," *Proceedings of ASME Turbo Expo 2006: Power for Land, Sea and Air*, American Society of Mechanical Engineers Paper GT2006-90128, 2006.

[23] Rao, K. V., Delaney, R. A., and Topp, D. A., "Turbine Vane-Blade Interaction: Vol. 1,2-D Euler/Navier-Stokes Aerodynamic and Grid Generation Developments," U.S. Air Force Research Lab. Rept. WL-TR-94-2073, Wright-Patterson AFB, OH, Jan. 1994.

[24] Sondergaard, R., Bons, J. P., and Rivir, R. B., "Control of Low-Pressure Turbine Separation Using Vortex Generator Jets," *Journal of Propulsion and Power*, Vol. 18, No. 4, July–Aug. 2002, pp. 889–895. doi:10.2514/2.6014

[25] Bons, J. P., Reimann, D., and Bloxham, M., "Separated Flow Transition on an LP Turbine Blade with Pulsed Flow Control," *2006 IGTI Conference*, International Gas Turbine Inst. Paper GT2006-90754, May 2006.

[26] "Davis Flowmaster," Ver. 7.0, LaVision GmbH, Gottingen, Germany, 2004.

[27] Volino, R. J., Schultz, M. P., and Pratt, C. M., "Conditional Sampling in a Transitional Boundary Layer Under High Free-Stream Turbulence Conditions," *Journal of Fluids Engineering*, Vol. 125, Jan. 2003, pp. 28–37. doi:10.1115/1.1521957

[28] Wu, X., and Durbin, P.A., "Evidence of Longitudinal Vortices Evolved from Distorted Wakes in a Turbine Passage," *Journal of Fluid Mechanics*, Vol. 446, Nov. 2001, pp. 199–228.

[29] Bloxham, M., Reimann, D., and Bons, J. P., "The Effect of VGJ Pulsing Frequency on Separation Bubble Dynamics," *AIAA 44th Aerospace Sciences Meeting and Exhibit*, AIAA Paper 2006-0876, Jan. 2006.

C. Tan
Associate Editor